JOURNAL OF SPACECRAFT AND ROCKETS
Vol. 37, No. 3, May–June 2000

Spaceborne Laser-Altimeter-Pointing Bias Calibration from Range Residual Analysis

S. B. Luthcke*
Raytheon ITSS, Greenbelt, Maryland 20771
David D. Rowlands†
NASA Goddard Space Flight Center, Greenbelt, Maryland 20771
John J. McCarthy‡ and Despina E. Pavlis§
Raytheon ITSS, Greenbelt, Maryland 20770
and
Eric Stoneking¶
Orbital Sciences Corporation, Beltsville, Maryland 20705

For many science applications of laser altimetry, the precise location of the point on the Earth's surface from which the laser energy reflects is required. The geolocation accuracy of this illuminated laser bounce point is primarily dependent on the accuracy of the laser-pointing knowledge. Laser and spacecraft body systematic misalignments are significant contributors to the pointing knowledge error. We present a method for accounting for these systematic misalignments through a Bayesian least-squares-estimation process using laser-altimeter range residuals. This range-residual calibration method uses commanded spacecraft attitude maneuvers and ocean range residuals for the recovery of the pointing and range biases. The performance of this method is evaluated through both consider-covariance and simulation studies applied to the upcoming Vegetation Canopy Lidar and the Ice and Cloud Elevation Satellite missions. The results of these analyses suggest arc-second level pointing bias knowledge can be achieved. A calibration maneuver is developed for both the Vegetation Canopy Lidar and the Ice and Cloud Elevation Satellite mission. The laser altimeter-range measurement model algorithm is presented.

Nomenclature

A = sine function amplitude, m for height and rad for angle
B = matrix of partial derivatives of the observations with respect to the parameters
C = angle bias parameter, rad
c = speed of light, m/s
D = cosine function amplitude, m for height and rad for angle
d = distance between current surface and bounce point estimate, m
$d\boldsymbol{m}$ = vector of residuals from the nth approximation
$d\boldsymbol{x}$ = differential correction to the estimated parameter value
F = exponential effective period, s
G = exponential coefficient, rad
h = height above surface, m
K = matrix of partial derivatives of the observations with respect to consider parameters
$\hat{\boldsymbol{n}}$ = nadir unit vector in local vertical local horizontal frame (LVLH)
P_N = noise-only covariance matrix
$\hat{\boldsymbol{p}}$ = laser pointing unit vector
R = rotation matrix
S = surface slope, rad
T = time tag, s
V_A = a priori parameter covariance matrix
V_S = a priori consider parameter covariance matrix
W = weighting matrix associated with the observations
$\boldsymbol{XB}$ = current estimate of surface bounce point position vector, m
$\boldsymbol{XCM}$ = center-of-mass offset vector for instrument optical tracking point, m
$\boldsymbol{XOP}$ = instrument optical tracking point position vector, m
$\boldsymbol{XS}$ = surface position vector at current bounce point estimate geodetic coordinates, m
$\boldsymbol{XSC}$ = spacecraft center-of-mass position vector, m
$\boldsymbol{x}$ = true state solution
$\boldsymbol{x}_A$ = a priori estimate of the true state solution
$\hat{\boldsymbol{x}}$ = approximation to the true state solution
Δt = time from maneuver or data start, s
$\Delta\boldsymbol{x}$ = error in the estimated parameters
$\Delta\rho$ = one-way range correction, m
θ = off-nadir angle, rad
ρ = range, m
σ_θ = standard deviation of the pointing angles, rad
σ_ρ = standard deviation of range, m
ω = angular frequency (2π/period), rad/s

Subscripts

atm = pertaining to atmospheric refraction
bias = pertaining to range bias
ECF = Earth-centered fixed frame
h = pertaining to height
IRF = inertial reference frame
Laser = laser frame
LVLH = local vertical local horizontal frame
p = pertaining to pitch
r = pertaining to roll
SBF = spacecraft body fixed frame
SBFC = spacecraft body fixed corrected frame
y = pertaining to yaw
2-way = roundtrip measurement
$\rightarrow$ = direction of rotation

Received 16 July 1999; revision received 7 February 2000; accepted for publication 8 February 2000.

*Principal Systems Engineer, Space Geodesy Branch, Code 926, NASA Goddard Space Center.
†Geophysicist, Space Geodesy Branch, Code 926.
‡Chief Scientist, Geodynamics, 7701 Greenbelt Road, #300. Member AIAA.
§Chief Programmer/Analyst, Geodynamics, 7701 Greenbelt Road, #300.
¶Senior Principal Engineer, TH02, 5010 Herzel Place.

Superscripts

B	= at bounce time
n	= iteration number
R	= at receive time
T	= at transmit time
T	= matrix transpose

Introduction

WITH two successful shuttle laser altimeter (SLA) missions (SLA-1 and SLA-2) (Ref. 1), the Mars Orbiting Laser Altimeter[2] and a host of aircraft experiments,[3,4] laser altimetry is revolutionizing the ability of remote sensing to determine the characteristics of complex surfaces including vegetation, slope, surface roughness, topography, and time variations. The laser-altimeter system measures the time of flight of the laser pulse and provides a digital time series of the returned laser pulse energy or the waveform. The time of flight determines the range to the surface bounce point, which in conjunction with the knowledge of the position and pointing of the laser altimeter enables the precise positioning or geolocation of the surface return. The waveform provides a detailed observation of the vertical distribution of intercepted surfaces within the laser footprint.[1] To exploit the unique observing capabilities of this technology, two NASA dedicated laser-altimeter missions are scheduled for launch in the very near future.

The Vegetation Canopy Lidar (VCL) mission, scheduled for launch in the later part of 2000, will carry a unique Multi-Beam Laser Altimeter (MBLA) instrument designed to observe vegetative canopy structure for a nominal mission duration of 1.5 years.[5] The VCL MBLA is a five-beam instrument where each laser is capable of producing returns with 30-m along-track spacing and 25-m-diam footprints when operating at 242 Hz. The five beams are oriented such that they produce an 8-km wide swath on the Earth's surface with each track separated by 2 km. VCL will orbit at an altitude of 400 km and an inclination of 67 deg. The Geoscience Laser Altimeter System (GLAS) will be launched aboard the Ice and Cloud Elevation Satellite (ICESat) in July of 2001.[6] The primary goals of ICESat are the measurement of ice sheet topography and temporal variations in addition to the characterization of cloud and atmospheric properties. The GLAS instrument possesses three lasers, each with an expected lifetime of 1.5 years, but will operate one laser at a time to provide an expected mission duration of 4.5 years. The GLAS laser footprint at the Earth's surface will be approximately 70 m in diameter with an along-track sampling distance of 175 m when operating at 40 Hz. ICESat will orbit at an altitude of approximately 610 km at an inclination of 94 deg.

The ground spot size of a spaceborne laser altimeter can be as small as the VCL footprint of 25 m and can be on the order of 20–80 times smaller than the footprint of a spaceborne radar altimeter now in use (TOPEX, GFO, ERS-2). The returned waveform provides detailed information about the surface characteristics within each footprint. The small laser footprints and the wealth of information they provide, over sometimes highly varying surface characteristics, require precise geolocation, typically on the order of the size of a footprint or less, which translates into approximately 13 and 22 arc-seconds (arcsec) in pointing for VCL and ICESat, respectively. Because identifying the spot that is illuminated is critical when utilizing laser altimetry, laser bounce point geolocation is a driving issue. Typically, laser-pointing errors are the dominant contributors to the geolocation errors. Pointing errors are certainly the dominant error sources for horizontal positioning and are significant contributors to height errors, especially in moderately to highly sloping terrain.[1,7] This is the case for VCL and ICESat, where the spacecraft positions will be known to less than 50-cm total position error, and the contributions from tracking point offsets and time tag errors have been minimized.[5,6]

The laser pointing with respect to the inertial reference frame (IRF) (typically J2000) is determined from 1) the spacecraft attitude knowledge, which gives the orientation of the spacecraft body fixed frame (SBF) with respect to the IRF and 2) the laser pointing with respect to the SBF. For VCL and ICESat a star tracker (ST) and gyroscope provide accurate knowledge of the spacecraft attitude. The pointing of the lasers and the orientation of the ST with respect to the SBF are measured prelaunch. However, misalignment biases are expected. The laser-detector coboresight alignment budgets for VCL and ICESat accommodate possible misalignments on the order of 30 arcsec. The overall pointing error will include the laser-detector coboresight misalignment and the misalignment of the laser-detector system with respect to the ST orientation. To understand the impact of these misalignment errors, we consider a 30-arcsec misalignment for a 400-km altitude instrument with a 1-deg laser-pointing surface incidence angle. The surface incidence angle includes the contributions from both surface slope and off-nadir pointing of the laser. In this case the misalignment will produce significant geolocation errors on the order of 58 m horizontally and 1 m in height. For a 600-km-altitude instrument the errors are 87 m horizontally and 1.5 m in height.

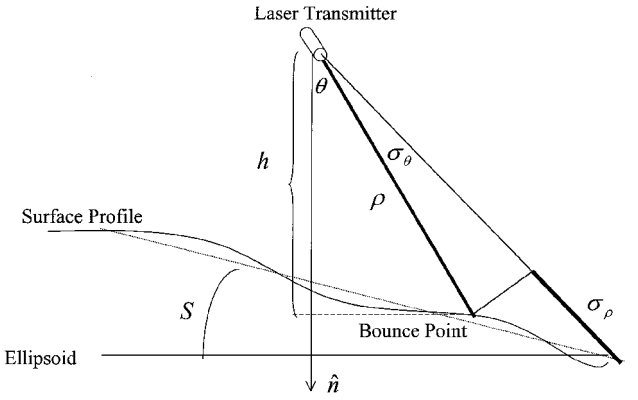

Fig. 1 Simple laser range geometry.

From the preceding discussion it is apparent that a method for estimating the pointing misalignment biases while on orbit is highly desirable. A simple representation of the laser range geometry can be found in Fig. 1. The sensitivity of the computed laser range to pointing errors can be simply expressed as

$$\sigma_\rho = \frac{h \tan(\theta + S)}{\cos(\theta + S)}\sigma_\theta \tag{1}$$

This relationship can be exploited for on-orbit calibration of the pointing misalignment biases. Attitude maneuvers in both roll and pitch can be used to observe three-dimensional pointing biases along with range bias. This technique has been used quite successfully with a simple iterative range minimization for both airborne and SLA data.[1,3,4] However, in this paper we present a formal implementation of the range-residual calibration technique for spaceborne laser-altimeter missions with VCL and ICESat as specific examples. A Bayesian least-squares batch estimation process is used to reduce the range residuals on successive iteration until convergence. The computed range and partial derivatives of the range with respect to the various estimable parameters are computed from a rigorous range measurement model. The range measurement model algorithm is presented in the Appendix. A calibration attitude maneuver is presented for application to both VCL and ICESat. The results of a detailed consider-covariance analysis and simulation are presented to gauge the performance of the range-residual calibration technique.

The range-residual calibration is the VCL mission's primary method to recover pointing misalignment biases. ICESat's primary method is a sophisticated stellar referencing system (SRS) that measures the orientation of the laser with respect to the ST to an accuracy of better than 1.5 arcsec (1σ). Even for ICESat the range-residual calibration technique provides a cost-effective method to independently verify the SRS observations and can be used as a backup in the event of an SRS failure.

Laser-Altimeter Range Processing

The geolocation of the laser surface return is computed from the laser-altimeter surface range observation along with the precise knowledge of the spacecraft position, instrument tracking points, spacecraft attitude, laser pointing, and observation times. The computed range is derived from a detailed measurement model algorithm using knowledge of the position, pointing and timing parameters,

along with surface height. The observed ranges are compared to those computed from the measurement model. The discrepancies between the observed and computed observations (i.e., the residuals) are minimized through the estimation of the parameters that affect the computed observation. For the laser range measurement model the bounce point location must be computed using some knowledge of the planet's surface. Although topographic models can be used, relatively flat, well-known surfaces such as lakes and oceans have been used to calibrate airborne and SLA pointing, respectively.[1,3]

To facilitate the processing of the laser-altimeter range data for the recovery of the model parameters, the laser-altimeter range measurement model algorithm has been implemented into NASA Goddard Space Flight Center's GEODYN precise orbit and geodetic parameter estimation system.[8] Therefore, the laser-altimeter range processing can take advantage of GEODYN's high-fidelity reference frame, detailed geophysical modeling, and its partitioned Bayesian least-squares-estimation process.[8] The GEODYN implementation allows for the simultaneous estimation of the geometric and dynamic parameters of the orbit and laser range measurement modeling through the reduction of a combination of spacecraft tracking and laser-altimeter range data. A detailed discussion of the direct altimeter range measurement model is provided in the Appendix.

Laser Pointing and Spacecraft Attitude Correction Parameterization

The pointing of the laser in the IRF is modeled with a succession of rotations, each denoted by R:

$$\hat{\boldsymbol{p}}_{\mathrm{IRF}} = R_{\mathrm{SBF}\rightarrow\ \mathrm{IRF}} R_{\mathrm{SBFC}\rightarrow\ \mathrm{SBF}} R_{\mathrm{Laser}\rightarrow\ \mathrm{SBFC}} \begin{bmatrix} 0 \\ 0 \\ -1 \end{bmatrix} \tag{2}$$

The time series of quaternions that represents the SBF-to-IRF rotations are provided by the postprocessed spacecraft attitude sensor data (ST and gyroscope). The first two rotation matrices, laser-to-SBFC (SBF corrected) and SBFC-to-SBF, are specified by the user with a three-axis Euler rotation in roll, pitch, and yaw. The Euler-angle representation was chosen because it is much more intuitive than a quaternion representation and, because the user has the flexibility to select the order of rotation, any singularities may be avoided. The SBFC-to-SBF matrix provides the capability to estimate a misalignment correction to the spacecraft attitude knowledge (SBF-to-IRF). GEODYN has the capability to model a laser-to-SBF rotation matrix for each of the N lasers that comprise the complete instrument (e.g., MBLA has five lasers). Only one SBFC-to-SBF matrix can be modeled. The laser-to-SBFC and the SBFC-to-SBF rotation matrices are constructed using roll, pitch, and yaw parameterized with a linear combination of terms. The functional forms of the various terms are selected to represent the expected laser and ST pointing variations as measured in the laboratory. The terms can be implemented as functions of time or telemetered temperature or pressure. For the purposes of this prelaunch error analysis, the parameterization shown in Eq. (3) was used to demonstrate the capability:

$$\begin{aligned} \text{roll} &= C_r + A_r \sin\omega\Delta t + D_r \cos\omega\Delta t - G_r(e^{-\Delta t/F_r} - 1) \\ \text{pitch} &= C_p + A_p \sin\omega\Delta t + D_p \cos\omega\Delta t - G_p(e^{-\Delta t/F_p} - 1) \end{aligned} \tag{3}$$

The parameterization is time dependent, which means the user can select different parameter sets for each distinct time period within a data-reduction arc. As many time periods (with user-defined length) as desired can be used. The partial derivatives of the direct altimeter range measurement with respect to each of the parameters of roll, pitch, and yaw (C, A, D, G, F) are computed by 1) rigorously computing the partials of the Euler angles with respect to the parameters and 2) chaining these partials with the numerically computed partials of the measurement with respect to the Euler angles.

The Euler angles for the SBF-to-SBFC and laser-to-SBFC cannot be simultaneously estimated. If the relative orientation of all of the lasers of an MBLA instrument were accurately known, then the three SBF-to-SBFC Euler angles would be sufficient to account for misalignment biases. Of course, the accuracy of the recovered SBF-to-SBFC alignment parameters would depend on the spatial orientation of the multiple lasers. However, the relative orientation of the five VCL lasers is not expected to be known to sufficient accuracy. Therefore, for the MBLA each laser must be treated independently with roll and pitch laser-to-SBF parameters estimated. These parameters will account for the total misalignment of each laser with respect to the telemetered spacecraft attitude. For the ICESat single-beam laser altimeter either set of Euler-angle parameters can be estimated. However, to remain consistent with the VCL case, the laser-to-SBF roll and pitch parameters will be used in the analysis presented next.

Calibration Maneuver

In addition to roll and pitch parameters, the estimation of range bias is very important because the pointing parameters are quite sensitive to range and height bias errors [Eq. (1)]. The recovered range bias accounts for both instrument range bias and height bias errors from various sources as will be discussed in the analysis sections that follow. A spacecraft attitude maneuver is employed to facilitate the simultaneous estimation of roll, pitch, and range bias parameters. The maneuver is a small, deliberate roll and pitch deviation of the spacecraft attitude from nominal nadir pointing, where the SBF z axis is pointing toward nadir. Both ICESat and VCL fly in a nadir-pointing local vertical local horizontal (LVLH) attitude with only two constant yaw (rotation about SBF z) regimes.[5,6]

The maneuver exploits the relationships found in Eq. (1). As the surface incidence angle is increased, the computed range error increases for a particular pointing error (Fig. 1). At the same time the contribution from a range bias remains constant and can be separated from the pointing errors. The maneuver isolates roll and pitch bias errors by either varying roll and pitch out of phase or sequentially. The size of the maneuver (size of the surface incidence angle) can be increased to observe smaller pointing bias errors. The ocean provides a well-modeled, relatively flat surface where the maneuver enhanced pointing error contributions to the range residuals can easily be observed.

The design of the maneuver must consider the duration of a typical ocean pass, the limits of the spacecraft attitude control system, the amplitude, period, and phasing sufficient to recover the desired bias accuracies, and any mission specific requirements. The maneuver is designed to fit within a typical ICESat and VCL 2070 s Pacific ocean track between ±60-deg latitude and use 1840 s of open ocean range data centered within the track. This scenario has the advantage of avoiding the increased ocean modeling and significant wave height errors at the higher latitudes and for ICESat will not disturb the fixed ground track at the high latitudes important for crossover observations of ice sheet topography. Additionally, the open or deep water (depths greater than 1 km) range data avoids ocean surface modeling complexities that arise at coastal boundaries.

The nominal maneuver presented here was specifically designed for VCL. However, the basic technique can be applied generally. The prelaunch assessment of the application of this maneuver to both VCL and ICESat are presented in the performance analysis next. Figure 2 shows the maneuver where roll and pitch are out of phase and varied with an amplitude of 3 deg to observe the roll

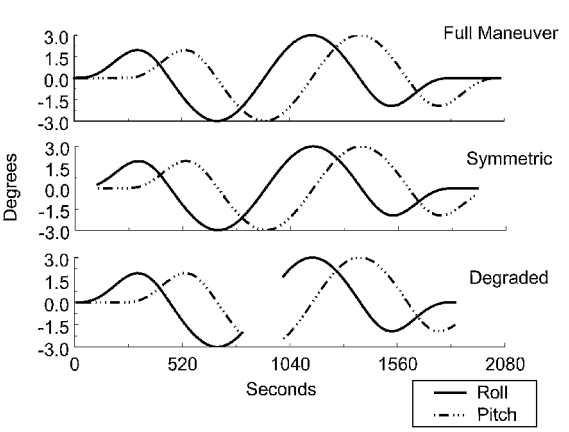

Fig. 2 Maneuver profiles.

and pitch bias errors. The full maneuver lasts the complete 2070 s, whereas the symmetric maneuver samples the ocean data only over a centered period of 1840 s. The out-of-phase technique is used rather than a sequential maneuver, where first roll is varied and then pitch, to shorten the length of time necessary for the maneuver without any loss in bias recovery performance. High frequency motion of the body must be avoided to allow the attitude knowledge system to suppress sensor noise maximally. The maneuver profile is thus a sinusoid with a frequency substantially lower than the attitude system bandwidth. At the beginning and end of the maneuver, a fairing function, continuous in the first and second derivatives, is used to transition smoothly from nadir pointing to the maneuver profile and back again.

The frequency of the maneuver is limited by the bandwidths of the attitude controller and the attitude knowledge system. In the case of VCL, the controller bandwidth is relatively low so as to avoid contributing to knowledge error. To allow the controller to track the maneuver command within operational pointing tolerances, the practical lower limit for the maneuver period is about 800 s. For the maneuver design presented here (Fig. 2) a period of 920 s is chosen, which is roughly $\frac{1}{6}$ of the orbit period. Therefore, one full-amplitude cycle can be completed within the 1840 s of observation time allowing for the fairing necessary for the maneuver start and stop. Additionally, aliasing with dominant once- and twice-per-orbit revolution errors (e.g., orbit position, timing, pointing) can be largely avoided with the higher frequency maneuver. Typically, the attitude knowledge bandwidth is more than a decade above the maneuver frequency (the case for VCL) so that maneuver motion contributes negligibly to knowledge error. The amplitude of the maneuver is limited primarily by the maximum angular rates developed because of sensor, torque, or momentum limitations. For VCL the slew rate is limited by growth of ST errors, resulting in a maximum amplitude of about 25 deg for an 800-s maneuver period. In practice, a modest 3–5 deg maneuver at 920 s is planned, which is well below system limitations.

During real operations data acquisition opportunities, editing and loss primarily caused by cloud cover will cause the maneuvers to be sampled in a nonoptimal manner. To understand and develop a realistic sampling model for the covariance and simulation analyses that follow, ocean surface return statistics from the SLA missions are used. The SLA instrument served as the engineering prototype for both ICESat and VCL, and therefore the instruments are quite similar in all important aspects including small footprint and wavelength.[1] SLA-02 operated at a 10-Hz data rate collecting data during 20 observation periods spanning a 10-day mission. The SLA-02 spaceborne laser-altimeter instrument collected over 50% of all possible ocean surface returns for both the midlatitude Pacific ocean and all oceans during its August 1997 mission. Similar results are observed for the January 1996 SLA-01 mission. Furthermore, the ocean tracks, including Pacific ocean midlatitudes, were well sampled with no significant continuous loss of data. Therefore, the analyses that follow model this resulting ocean surface sampling by 1) employing a data rate that represents 50% data loss or greater (e.g., 5 Hz for the covariance analysis and 2 Hz for the simulations) and 2) employing a degraded maneuver with a long continuous loss of data. The VCL will operate between 10 and 242 Hz, whereas the ICESat GLAS instrument will operate at 40 Hz continuously.

Several degraded maneuver scenarios were constructed. The maneuvers were started such that the sampling was not symmetric, and a ~200 s segment of data was deleted. The missing segment of data was moved around such that it cut off a peak of the roll, a peak of the pitch, and fell between peaks of roll and pitch. Figure 2 shows the case where data at a peak of the pitch maneuver was deleted (labeled degraded). For each of the cases studied, the resulting degradation in the root sum square (rss) of the pointing bias error was approximately the same. When data at the pitch peak were deleted (Fig. 2), the recovered pointing bias degradation occurred primarily in the recovered pitch bias, as would be expected. The combination of both a significantly lower sampling rate and the degraded maneuver results in data loss much greater than that observed by SLA and provides a conservative model for our prelaunch error analysis. Furthermore, the calibration maneuvers can be performed regularly during the mission (e.g., every seven days) and quite frequently (e.g., every day or more) during on-orbit "check out." Therefore, the data from all maneuvers can be summed together in the estimation process to provide for a well-sampled roll and pitch maneuver.

Performance Analysis Methodology and Error Models

A VCL and ICESat prelaunch performance analysis has been performed to gauge the accuracy of the recovered biases using the range-residual calibration technique just described. The biases are estimated from the range residuals assuming Bayesian least-squares differential correction estimation in a batch processing mode.[8] Both consider-covariance error analysis and simulations have been employed to assess performance independently. The covariance analysis provides an estimate of the errors in the adjusted parameters from the noise-only covariance and from errors in unadjusted or "consider" parameters. Therefore, the covariance analysis provides a statistical understanding of the expected performance. The simulations give a direct indication of how well the pointing can be recovered. The recovered pointing is compared to the truth pointing that was used to generate the simulated laser-altimeter range observations. The simulation analysis is limited by the fact that each simulation represents the performance for a specific ensemble of errors. Therefore, it is important to have both a statistical understanding of the errors from the covariance analysis and a specific example from the simulations.

Both the covariance analysis and the simulations use a differential correction Bayesian least-squares estimation. The estimated parameters are solved for iteratively. The differential correction to the estimated parameter value (true solution approximation) on the nth iteration is given by the Bayesian parameter estimation formula[8]:

$$\mathrm{d}\boldsymbol{x}^{(n+1)} = \left(B^T W B + V_A^{-1}\right)^{-1}\left[B^T W\, \mathrm{d}\boldsymbol{m} + V_A^{-1}\left(\boldsymbol{x}_A - \hat{\boldsymbol{x}}^{(n)}\right)\right] \quad (4)$$

The estimate of the state after the $n + 1$ iteration is given by

$$\hat{\boldsymbol{x}} = \hat{\boldsymbol{x}}^{(n)} + \mathrm{d}\boldsymbol{x}^{(n+1)} \quad (5)$$

The error in the estimated parameters is then given by

$$\Delta \boldsymbol{x} = \hat{\boldsymbol{x}} - \boldsymbol{x} \quad (6)$$

The partial derivatives of the range are needed with respect to the various parameters to be estimated and considered for the performance analysis. Additionally, the observed and computed ranges must be constructed for the simulations. When processing real range data, the rigorous measurement model described in the Appendix is needed to calculate the computed range, which is then differenced with the observed range to form residuals. However, for a realistic performance analysis it is only important that our residuals reflect realistic errors of commission and omission in the computed ranges. Certain effects like the motion of the satellite during the round trip time of the laser pulse are in practice accurately modeled and do not contribute significant errors of commission in real residuals. Therefore, our performance error analysis does not need to use a range measurement model, which considers the time of flight of the satellite, or any other effect, which is usually well modeled. The expression for the simplified computed range, which considers all of the important sources of error commission, is presented in Eq. (7). This expression is easy to evaluate and allows us to run many test cases with relatively little computational burden. Even so, it allows our performance analysis to consider any type of commission error structure arising from our lack of knowledge of the surface.

$$\rho = h/\left(R_{\mathrm{SBF}\rightarrow \mathrm{LVLH}} R_{\mathrm{SBFC}\rightarrow \mathrm{SBF}}\, \hat{\boldsymbol{p}}_{\mathrm{SBFC}}\right)\hat{\boldsymbol{n}} \quad (7)$$

$$\hat{\boldsymbol{p}}_{\mathrm{SBFC}} = R_{\mathrm{Laser}\rightarrow \mathrm{SBFC}} \begin{bmatrix} 0 \\ 0 \\ 1 \end{bmatrix} \quad (8)$$

The laser pointing in the SBF consists of only a roll and pitch because the laser pointing in the laser frame is assumed to be in the z direction. For VCL the nominal laser pointing is 10 mrad from

the SBF z axis, whereas for ICESat the nominal laser pointing is assumed to be along the SBF z axis. The SBF-to-LVLH rotation represents the maneuver, whereas the SBFC-to-SBF provides for body misalignment error modeling and parameterization.

The laser-to-SBFC and SBFC-to-SBF Euler-angle biases, range bias, and height parameters (slope, periodic, bias) can be estimated or used as consider parameters in the covariance analysis. For the consider-covarianceanalysis, range and laser-to-SBF roll and pitch Euler-angle biases are always estimated unless otherwise noted. The laser-to-SBF angle biases account for SBF misalignment biases and misalignment of the laser pointing with respect to the SBF. Therefore, there is no effective contribution from the SBFC-to-SBF angle bias errors when considering resultant pointing error in the measurement model frame. Periodic height (contribution from surface and spacecraft position) errors are modeled as

$$\text{periodic height} = A_h \sin \omega \Delta t + D_h \cos \omega \Delta t \tag{9}$$

The amplitude of the sine and cosine functions (A_h and D_h) are the parameters that can be estimated or considered. The frequency is varied to investigate the effect from a periodic height error over a broad spectrum. The laser variations are modeled as given by Eq. (3). The total amplitude of the periodic height variation expressed in Eq. (9) is the rss of the sine and cosine amplitudes. The amplitude of the total periodic pointing variation, as expressed in Eq. (3), is the rss of the total roll and total pitch periodic term amplitudes.

Consider-Covariance Analysis Details

From Eqs. (4) and (6) the total error covariance matrix of the adjusted parameters is given by[9]

$$E[(\Delta \boldsymbol{x})(\Delta \boldsymbol{x})^T] = P_N + \left(P_N B^T W K\right) V_S \left(P_N B^T W K\right)^T \tag{10}$$

The first term is the no-model-error or noise-only covariance given by

$$P_N = \left(B^T W B + V_A^{-1}\right)^{-1} \tag{11}$$

The second term is the contribution from the uncertainty in the unestimated or considered parameters. The standard deviations of the estimated parameters are then computed by taking the square root of the diagonal terms of the total error covariance matrix.

Table 1 presents the various contributions to the range measurement variance used to construct the observation weight matrix W in Eq. (10). For this analysis the weight matrix is simply the identity matrix multiplied by the inverse of the range variance. The first five contributions in Table 1 were computed using the expressions found in Gardner[7] and the system details outlined in Table 2. The system effects include the contributions from the outgoing pulse width, the number of effective bits, and the A/D sampling interval. The surface incidence angle effect includes the contribution from the beam divergence or the footprint diameter. The body attitude knowledge jitter represents the postprocessed error not including the misalignment biases.

Table 1 Covariance analysis 1σ range error (assume 3-deg slope)

Contribution	VCL, cm	ICEsat, cm
System effects	19	7
Laser-pointing jitter	31	15
Body attitude knowledge jitter	51	38
Surface incidence angle (footprint)	4	11
Surface roughness	6	6
Radial orbit	15	5
Horizontal orbit	3	1
Atmospheric delay	<5	<1
Transmit and receive point relative to spacecraft center of mass	4	0.5
Time tag	<1	<1
Ocean surface modeling		
RMS surface from waves	150	150
SST	11	11
Ocean tides	3	3
Earth tides	<1	<1
Atmospheric pressure loading	1	1
RSS	164	157

Table 2 System details

Characteristic	VCL	ICEsat
Altitude and inclination	390–410 km/67 deg	593–623 km/94 deg
Surface footprint diameter/laser	25 m	70 m
Along-track shot spacing/laser	30 m (land)	175 m
Data frequency/laser	10–242 Hz	40 Hz
Pulsewidth (full width half max)	10 nsec	6 nsec
Detector type	Si APD	Si APD
A/D sampling interval	250 MHz	1000 MHz
Effective bits	8	7
Laser-pointing jitter (1σ)	3 arcsec	1 arcsec
Body attitude knowledge jitter	5 arcsec	2.5 arcsec
1σ horizontal orbit error	50 cm	20 cm
Observation time tag with respect to global positioning system	10 μs	10 μs

The contribution from surface waves is an important aspect to be considered in the error model. However, a detailed surface wave error model would be quite complex and beyond the scope of this paper. Therefore, we have attempted to sufficiently account for surface wave-induced range errors by modeling the contribution as random normal with an appropriate standard deviation. Any biasing that would occur because of the real shape of the surface waves (e.g., trichoidal) and the footprint sampling of the surface wavelength scales is considered as height bias errors and removed through the range bias estimation. Any long wavelength variation of the bias is considered in the periodic and slope height error modeling discussed in the analysis presented in the following sections. The surface roughness component (Table 1) is computed at a 3-deg surface incidence angle conservatively considering all of a 1-m wave surface root mean square (rms) is within the footprint. The average significant wave height (SWH) can be estimated from data produced by the National Center for Environmental Prediction (NCEP) and is available on their web site. Both the NCEP global ocean models and the maps of SWH derived from ERS-2 data give approximately 2-m rms SWH in calm, storm-free oceans in the midlatitudes.[10] Kraus and Businger[11] quote an analysis by Longuet-Higgins that relates SWH to the sea-surface variance. From this relationship the rms sea-surface height should be about 0.7–1.0 m, given a SWH of 2.0 m. As seen in Table 1, a wave-induced rms surface height of 1.5 m is conservatively used. For significant wave heights between 1.3 and 3.7 m, the surface elevation distribution is well modeled by a Gaussian.[12]

Estimates of the error in modeling the sea-surface topography (SST) are derived from Yi[13] and Wunsch and Stammer.[14] Although this error is applied to the range variance assuming a Gaussian distribution, the error is also applied as a systematic contribution at various frequencies as discussed in the Consider-Covariance Analysis section. An ocean surface modeling height bias error will be accommodated through the estimation of a range bias as will be presented in the next analysis. Comparison of the Topex/Poseidon ocean tide models with the Schrama and Ray model gives an rms difference of about 3 cm (Ref. 15). The error in the displacement caused by Earth's tides is less than 1 cm (Ref. 16). The response of the ocean surface caused by atmospheric pressure loading must also be considered. The open ocean response can mostly be accommodated by a simple inverted barometer (IB) correction, where the change in height is related to the deviation in pressure from a standard atmosphere by -0.995 cm/mbar (Ref. 17). For much of the open ocean maneuver path, the rms variability of atmospheric pressure is less than 10 mbar (Ref. 17). Although this effect is not large, much of it (90–95%) can be accommodated using sea-level atmospheric pressure model data provided from a center such as the European Center for Medium-Range Weather Forecasting (ECMWF) and the simple IB correction (Koblinsky, C. J., "Reprocessing of Altimeter Data for Oceanography," NASA/GSFC Ocean Pathfinder, URL: http://neptune.gsfc.nasa.gov/ocean.html; cited 19 January 2000). The atmospheric delay of the laser is dominated by the dry tropospheric refraction term, where pressure errors of 1 mbar produce range errors on the order of 2 mm. Using a standard atmosphere and

assuming that the data are edited to include near clear sky conditions, the probable correction error is about 3 cm. With proper modeling of the atmospheric surface pressure and temperature (e.g., ECMWF surface pressure and temperature data), subcentimeter level correction accuracy can be achieved. The change in the correction caused by off-nadir pointing is minimal with a 3-mm range change for a 3-deg off-nadir pointing. However, this assumes application of the nadir correction to all points in the maneuver. In practice, we will apply the correction taking into account the off-nadir angle. Therefore, the error in the dry troposphere correction will be much smaller.

Simulation Analysis Details

The simulation analysis provides an assessment of how well the pointing biases can be recovered from laser-altimeter observations. To accomplish this, the simulations must have a realistic error model. Any realistic error model will differ from the errors that can be produced by the parameters in the measurement model used to form the computed observations. The additional error content is caused by omission of effects, which are impossible or impractical to model or by commission errors in the measurement model itself.

Table 3 summarizes the sources of the additional error content in our simulated observations. The ST errors in Table 3 are presented in the SBF frame to be consistent with the other pointing error sources. The ST error model was derived from internal VCL design review and represents the current (at the time of this writing) expected level of performance after postprocessing of the data. The ST error model was computed in the ST frame considering the following contributors: line-of-sight uncertainty, centroiding, noise equivalent angle, catalog, chromaticity, ground calibration, thermal scale, point spread function distortion, and optical distortion. Both VCL and ICESat will fly state-of-the-art STs with similar expected performance. Therefore, for the purposes of the simulations the ST error model was used for both the VCL and ICESat body attitude error models with the difference being the orientation of the ST with respect to the SBF, as noted in Table 3. The ST frame yaw is a rotation about the ST boresight, and roll and pitch complete a right-handed orthogonal system. The spacecraft body z axis is pointed toward nadir while the instrument is pointed nearly along this axis (VCL lasers oriented 10 mrad from z and ICESat assumed pointed along z). The geolocation is therefore very sensitive to SBF roll and pitch errors. The ST contribution to the SBF errors depends on the orientation of the ST boresight within the SBF because the ST boresight (yaw) errors are greater than the roll and pitch errors. The standard deviation and mean of the simulated ST errors rotated to the SBF are provided in Table 3 for both VCL and ICESat.

The simulation error model includes the various components of the expected pointing errors (Table 3). The laser-pointing jitter is modeled as a random normal process with the prelaunch expected standard deviation. The misalignment biases model the effects of prelaunch measurement error, launch stresses, and gravity relaxation once on orbit. The thermal variations attempt to model the mechanical change in pointing caused by environmental and operational temperature changes. The effects of periodic, slope, and bias height errors are included along with waves and instrument noise and range bias (Table 3). The error model summary provided in Table 3 represents a preliminary system performance estimate and does not necessarily represent the final on-orbit performance.

Performance Analysis Results

Consider-Covariance Analysis Results

Pointing bias accuracy, recovered using the attitude maneuvers already described, is strongly dependent on range bias. Increasing the amplitude of the maneuver can significantly reduce the impact of range bias. However, the impact can be reduced even more, still keeping a small maneuver amplitude. For VCL the lasers are pointed 0.01 rad or 0.58 deg from the SBF z axis, and therefore they are nominally oriented 0.58 deg off of nadir. This orientation imparts a constant surface incidence angle that magnifies the pointing bias error sensitivity to range or height bias. To compensate for this, the maneuver can be performed such that the ocean range data are sampled evenly on either side of nadir. In other words, the maneuver is modified to mimic the case where the laser is oriented with a 0-deg z offset. This technique works quite well in reducing the impact of

Table 3 Simulation error model summary (preliminary system performance)

Contribution	VCL	ICEsat
Body attitude errors		
Spacecraft jitter	1.00 arcsec random (1σ)	
ST errors in SBF[a]	Roll and pitch: σ = 4.56 arcsec mean = 3.25 arcsec Yaw: σ = 1.62 arcsec mean = −2.40 arcsec	Roll and pitch: σ = 2.02 arcsec mean = 1.67 arcsec Yaw: σ = 4.42 arcsec mean = 3.56 arcsec
Smoother	Roll and pitch: 1.70 arcsec random (1σ) Yaw: 0.47 arcsec random (1σ)	
Velocity abberation	Roll, pitch, and yaw: 0.10 arcsec bias	
Coordinate frame	Roll, pitch, and yaw: 0.50 arcsec bias	
Misalignment bias	Roll: 450 arcsec, pitch: −300 arcsec, yaw: 1000 arcsec	
Laser-pointing errors		
Jitter	3.00 arcsec random (1σ)	2.00 arcsec random (1σ)
Thermal variations		
Periodic amplitude	Roll, pitch (each): 7 arcsec	Roll, pitch (each): 30 arcsec
Period	5520 s	5520 s
Exponential amplitude	Roll, pitch (each): 30 arcsec	Roll, pitch (each): 0 arcsec
Effective period	300 s	300 s
Misalignment bias	Roll: 30 arcsec, pitch: 100 arcsec	
Height errors		
Periodic amplitude	27 cm	17 cm
Period	920 s (worst case, period of maneuver)	
Slope	50 cm total rise over maneuver	
Bias	1 m	
Waves/random	1.5 m random (1σ)	
Range		
Instrument noise	20 cm random (1σ)	10 cm random (1σ)
Range bias	1 m	

[a]Standard deviation and mean of ST error model rotated from the ST frame to the SBF (VCL ST-to-SBF: roll = 180 deg, pitch = −75 deg, yaw = 161 deg; ICEsat ST-to-SBF: roll = 180 deg, pitch = 0 deg, yaw = 0deg).

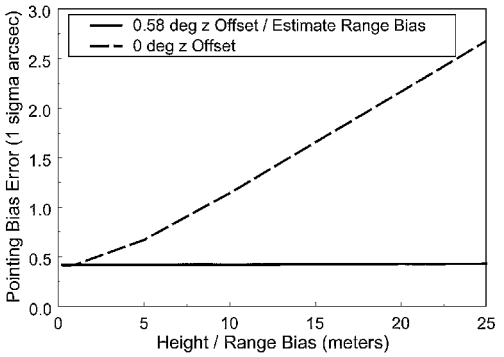

Fig. 3 Recovered pointing error dependence on height/range bias (400-km altitude, 5-Hz data, 3-deg maneuver).

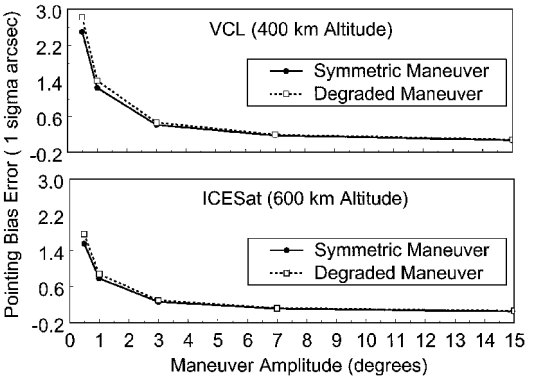

Fig. 4 Recovered pointing error dependence on maneuver sampling (5-Hz data, 1-m height bias, estimate range bias).

range bias (Fig. 3) and has been used successfully in processing of airborne data.[3,4]

The preceding technique is impractical for an MBLA instrument like VCL. A separate spacecraft maneuver would have to be performed for each laser because the lasers are each oriented differently around a cone making a 0.58-deg angle with the body z axis. Instead, a range bias is simultaneously estimated for each of the lasers along with the pointing bias parameters. A comparison of the resultant VCL laser pointing bias error for the 0-deg z offset technique (estimating only pointing biases) with estimating a range bias together with pointing, both using a 3-deg maneuver, is presented in Fig. 3. The pointing bias error is shown as a function of considered height or range bias error. The error in the estimated pointing bias is the rss of the errors in the estimated roll and pitch biases. The results show that the effects of the constant surface incidence angle imparted by the laser off-z-axis orientation are inconsequential when estimating a range bias parameter, and no special maneuver for each laser orientation is necessary. A single maneuver provides for the separability of the pointing and range bias, and this is the approach that will be used on orbit for VCL.

From the expression for the computed range [Eq. (7)], one can see that a range bias can account for a height bias error (orbit or surface modeling) for small off-nadir angles. The partial derivative of the computed range with respect to the range bias is equal to one, whereas the height bias partial derivative is the reciprocal of the cosine of the off-nadir pointing angle. Even for 10-deg maneuvers, these partial derivatives differ by only 2%. For reasonable ocean surface modeling performance, where ocean topographic height uncertainty is well below a meter and considering a 3-deg amplitude maneuver, estimating a range bias accounts for the height bias error and the effects of the off-z-axis laser orientation. In fact, Fig. 3 shows that estimating a range bias can easily accommodate the effects of height bias error up to at least 25 m even in the presence of 0.58-deg off-z-axis pointing.

The covariance analysis was used to select a maneuver amplitude for the VCL and ICESat cases. A 1-m (1σ) height bias error was considered while the pointing and range bias parameters were estimated. Figure 4 shows the recovered pointing bias error as a function of maneuver amplitude using both the degraded and symmetric maneuver profiles just presented (Fig. 2). In an effort to minimize the maneuver, the 3-deg amplitude is selected. At 3 deg the curves begin to level off, and the results show 1σ sub-arcsec level pointing bias recovery is possible. A comparison of the VCL and ICESat results shows the increased ICESat pointing bias performance primarily caused by the greater lever arm from the increased altitude. The impact of the degraded maneuver on recovered pointing bias performance is also presented in Fig. 4. The performance degradation is minimal, with recovered pointing bias error increasing only by a factor of approximately 1.13.

Up to this point in the covariance analysis, we have included a very simple height (surface and orbit) error model, which only considered the effects of a constant height bias error and random normal contributions to the range variance from various error contributors (Table 1). We also studied the impact of considering both systematic slope and periodic height errors. These height errors account for errors in modeling the SST and surface wave sampling induced height bias variations. The results show that even considering extremely large slope errors that amount to 10-m height errors over the distance of the maneuver the pointing biases can be resolved to a few arcseconds. The long wavelength temporal variations that would manifest themselves as a systematic sea-surface slope error over the period of the maneuver are only on the order of a few centimeters.[14] Therefore, the pointing bias calibration is negligibly affected by slope height errors in ocean surface and orbit modeling.

The error in the height modeling is primarily caused by radial orbit errors, errors in modeling the ocean topography, and bias variations from sampling surface waves. The contribution from radial orbit error is expected to be on the order of 5 and 15 cm rms for ICESat and VCL respectively as has been just discussed (Table 1). We now assume the SST will be simply modeled using a gridded mean sea-surface model (geoid and dynamic ocean topography) such as OSU95 and an ocean tide model such as the Schrama and Ray model.[13,18] The altimeter data are edited to include only deep oceans with depths greater than 1 km to eliminate large modeling errors near the coasts, and all of the usual ocean surface corrections are assumed to be made (e.g., IB, solid Earth tides). The model errors and the unmodeled temporal variations in the SST will then constitute our surface height modeling errors. Ocean-wide comparisons to Topex-observed sea-surface height observations indicate this approach can model the ocean surface to better than 11 cm (1σ) (Ref. 13). If we edit the data for the major western coastal boundary currents, the error will be further reduced. Additionally, observations of the temporal variations in the ocean surface for two years of Topex data and a 10-day snapshot support this as a conservative estimate of sea-surface modeling error.[14] Therefore, we construct a height modeling error estimate through the rss of the radial orbit error and the sea-surface height modeling error. The estimated height modeling error for VCL is then 19 cm (1σ) and 12 cm (1σ) for ICESat.

The impact of periodic height modeling error is presented in Fig. 5. The periodic height error is introduced using the expression in Eq. (9) where the amplitude of the sine and cosine functions are the consider parameters. Figure 5 shows the recovered pointing bias error as a function of the period for three different total amplitudes of the periodic variation. The 3-deg degraded maneuver was used with a 1-m (1σ) height bias and a 50 cm (1σ) total rise slope height error applied in addition to the periodic error. A range bias was estimated along with the pointing biases. Again, the contributions to the range variance outlined in Table 1 are applied. For periodic height errors with periods less than 200 s and greater than 3100 s, the recovered pointing bias error has a contribution of less than 0.5 arcsec (1σ) for both VCL and ICESat. Therefore, sea-level variations with spatial scales less than 1400 km, such as mesoscale eddies (50 km) and coastal boundary current meanders (500 km), will have a negligible effect. The maximum pointing bias error occurs for sinusoidal height errors with a period equal to the maneuver period and peaks at $\frac{1}{2}$ and $\frac{1}{4}$ the maneuver period can be observed (Fig. 5).

We now assume the worst case where all of the height modeling error manifests itself as a sinusoidal variation at the maneuver

Table 4 Covariance analysis summary (5-Hz data rate)

	Pointing bias error (1σ arcsec)	
Case	VCL	ICESat
3-deg degraded maneuver	3.1	1.3
5-deg degraded maneuver	1.9	0.8

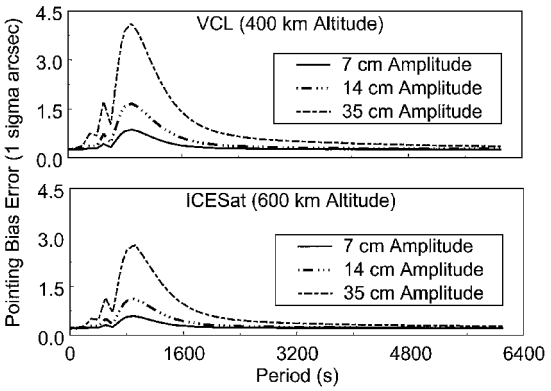

Fig. 5 Recovered pointing error dependence on periodic height error including 50-cm slope error (degraded maneuver, 1-m height bias, estimate range bias).

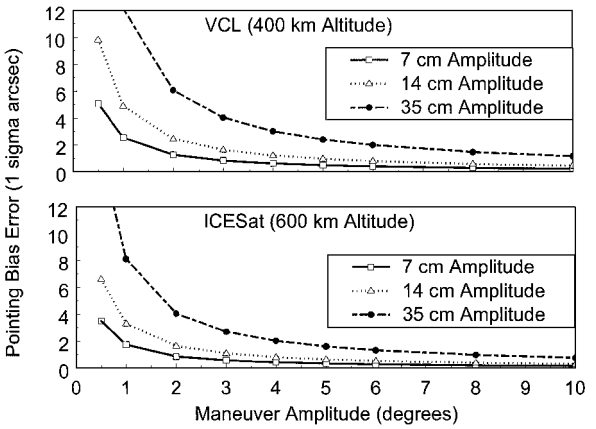

Fig. 6 Pointing error dependence on maneuver amplitude including periodic and 50-cm slope height error (degraded maneuver, 1-m height bias, estimate range bias).

period. This conservative approach is taken to account for the possibility of long wavelength bias variations caused by the sampling of the surface waves. The 19 cm (1σ) of VCL expected height modeling error is then considered to be a 27-cm amplitude sinusoidal height error with period 920 s because the standard deviation of a 27-cm amplitude sine function is approximately 19 cm. For the 12 cm (1σ) of ICESat error, a 17-cm amplitude is considered. Using this worst-case height modeling error (including the 1-m height bias and 50-cm total rise slope height errors), the VCL and ICESat recovered pointing bias errors are found to be less than 3.1 and 1.3 arcsec (1σ) respectively for a 3-deg degraded maneuver (Table 4). Estimation of the range bias accounts for both range and height biases with an uncertainty of less than 4 cm. These results are valid for both high and low repetition rates because they are dominated by the consider parameter error. Figure 6 presents the recovered pointing bias error as a function of maneuver amplitude for the worst-case height modeling error just discussed. For a 5-deg degraded maneuver the VCL and ICESat recovered pointing bias errors are found to have uncertainty estimates of less than 1.9 and 0.8 arcseconds (1σ), respectively.

Simulation Analysis Results

In addition to the covariance analysis just shown, simulations were performed. The simulations assume a 3-deg amplitude degraded maneuver. Range residuals were simulated for both VCL and ICESat using the error models just discussed and summarized in Table 3. The worst-case height error is modeled with the various parameters outlined in Table 3 and just discussed. The periodic height error is modeled in phase with the maneuver and at the period of the maneuver.

At the time of this writing, the exact dependence of pointing on temperature is not known. However, to complete the detail of these simulations we include an estimate of this contribution. Therefore, we make the following assumptions to devise our error model and method of recovery. First, we assume that prelaunch the pointing variation as a function of temperature will be measured and mathematically characterized for implementation into the measurement model. We then assume that we will need to tune this prelaunch pointing variation model postlaunch by adjusting appropriate parameters of the model with laser range data. The parameters will represent the size (amplitude) and direction (roll and pitch) of the pointing variation as a function of temperature. Therefore, the actual functional representation of the pointing variation is not important, but the ability to tune the model is. To demonstrate this capability, the thermal variations are modeled using the periodic and exponential terms found in Eq. (3) and the parameter values outlined in Table 3. The amplitude of the periodic and exponential terms are chosen so that the variation is on the order of the current VCL and ICESat instrument coboresight budget (~30 arcsec).

The VCL laser transmitter thermal pointing variations will likely be dominated by the operational scenario where the instrument is turned on (242 Hz) for land and turned off (10 Hz) for ocean. Therefore, the thermal variation is modeled primarily as the exponential term found in Eq. (3) with an amplitude of 30 arcsec on both roll and pitch and a 300-s effective period. A once-per-orbit revolution periodic variation with an amplitude of 7 arcsec on both roll and pitch is modeled to mimic possible environmental contributions. The following parameters are then considered for estimation [see Eq. (3)]: range bias, roll and pitch bias (C_r, C_p), roll and pitch exponential amplitude (G_r, G_p). Longer wavelength variations that would depend on the orientation of the orbit plane with respect to the sun can be recovered from adding together the normal equations from several maneuvers sampling this variation.

The ICESat laser is continuously operating at 40 Hz. We can expect the thermal pointing variations to be dominated by the orientation of the instrument with respect to the sun. Therefore the pointing variation is modeled as the periodic terms in Eq. (3) with a roll and pitch amplitude of 30 arcsec and a period equal to the orbital period of the spacecraft. The following parameters are then considered for estimation [see Eq. (3)]: range bias, roll and pitch bias (C_r, C_p), roll and pitch sine and cosine coefficients (A_r, A_p, D_r, D_p). Again, the important point is to demonstrate the ability to tune a pointing variation model and not the actual functional form of the pointing variation itself. The simulations were performed with a 2-Hz data rate to ease computational burden.

The VCL range residuals from the simulation are presented in Fig. 7. It is important to maximize the observability of the exponential pointing variation 300-s effective period. Therefore, the VCL lasers are deliberately turned on 450 s from the start of the maneuver. In this way the 300-s effective period is observed at the maximum transitions of the maneuver. Again, a 3-deg degraded maneuver was used in the simulations where the data are missing at one of the peaks of the maneuver (Fig. 7). Figure 7 shows the range residuals from three VCL simulations: 1) no parameter estimation, 2) estimate range bias and roll and pitch bias (C_r, C_p) and 3) estimate range bias, roll and pitch bias (C_r, C_p), and roll and pitch exponential coefficients (G_r, G_p). A statistical summary of the range residual and pointing results is provided in Table 5. The remaining range residual 1.58 m rms is dominated by the random normal component of our surface wave error model. The pointing bias is derived by 1) first computing the mean pointing vector for both the simulated truth and the modeled pointing performing a center-of-mass computation where the mass or weighting is 1, 2) then the bias is the

Table 5 Simulation analysis summary (2-Hz data rate, 3-deg degraded maneuver)

Case	Pointing		Range residual
	Bias, arcsec	rms, arcsec	rms, m
VCL			
No estimate	519.6	519.2	27.22
Estimate roll, pitch, and range bias	6.0	12.8	1.64
Estimate range bias and roll, pitch (each): bias and exponential coefficient	3.0	8.1	1.58
ICESat			
No estimate	533.9	534.0	43.26
Estimate roll, pitch, and range bias	5.7	13.1	1.71
Estimate range bias and roll, pitch (each): bias and sin + cos coefficient	1.4	5.0	1.54

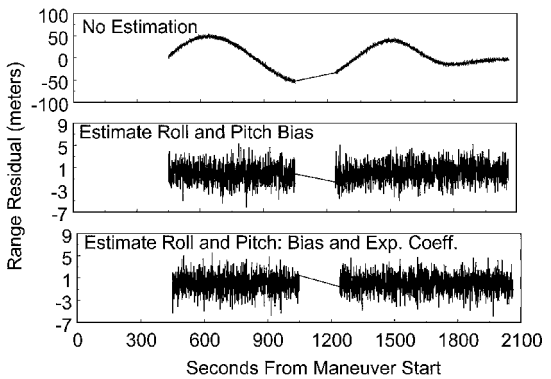

Fig. 7 VCL simulation range residuals.

angle between the simulated truth and modeled mean pointing vectors computed using a dot product. The analysis demonstrates the ability to estimate pointing variation model parameters in addition to the range, roll, and pitch biases. Both the size and the direction of the pointing variation have been estimated. The simulation shows that the VCL laser pointing bias can be estimated at the 3-arcsec uncertainty level for a 3-deg degraded maneuver. These results are in agreement with the covariance analysis results presented in Table 4.

Similar results were obtained for ICESat using a 3-deg degraded maneuver. A statistical summary of the ICESat simulation results is provided in Table 5 for the cases: 1) no parameter estimation, 2) estimate range bias and roll and pitch bias (C_r, C_p) and 3) estimate range bias, roll and pitch bias (C_r, C_p), and roll and pitch sine and cosine coefficients (A_r, A_p, D_r, D_p). The analysis again demonstrates the ability to estimate pointing variation model parameters. The size, direction, and phase of the pointing variation have been recovered in addition to the range, roll, and pitch biases. The simulation demonstrates that the ICESat laser pointing bias can be estimated at the 1.4-arcsec uncertainty level for a 3-deg degraded maneuver. Again, these results are in agreement with the covariance analysis results presented in Table 4.

Conclusion

The advent of a new generation of remote sensing satellites equipped with laser altimeters is providing a wealth of data for a broad spectrum of scientific investigations. The geolocation accuracy of the laser surface return is an important aspect in the application of the data. Mission requirements for many applications require geolocation accuracy be within a footprint. Systematic misalignments of the body attitude and the laser pointing are significant contributors to geolocation error. Because the errors in mounting the ST and lasers and the characteristics of the instrument will probably change because of the stresses of launch, on-orbit calibration of pointing biases will be necessary. As the missions progress and the satellite components age, it is possible that these biases will also change, thus requiring periodic, on-orbit recalibrations.

The range-residual calibration method presented in this paper is well suited to the requirements of such on-orbit calibrations. Easily implemented attitude maneuvers, which are small deviations from the nominal attitude profile, have been developed to support the recovery of the pointing and range biases over a short 2070-s calibration maneuver. For the satellites considered VCL and ICESat, the maneuvers can be performed over midlatitude oceans when the primary mission observations (vegetation and ice sheet change observations) are not being acquired. Additionally, the algorithm for the laser-altimeter range measurement model has been developed and presented. The measurement model has been implemented into the GEODYN orbit determination and geodetic parameter estimation system to take advantage of GEODYN's precise geodetic and reference frame modeling along with the partitioned Bayesian least-squares differential correction estimation scheme. The various parameters (including pointing and range biases) that make up the laser-altimeter range measurement model can be estimated from the simultaneous reduction of spacecraft tracking and laser-altimeter range data types.

Both consider-covariance analysis and simulations were used to gauge the performance of this on-orbit calibration method. The covariance analysis provides a statistical summary of the performance that can be compared to specific simulation cases using detailed error models. The analysis presented in this paper demonstrates that the range-residual analysis on-orbit calibration method can be expected to achieve arcsecond-level pointing bias knowledge for spaceborne laser-altimeter missions such as VCL and ICESat. In particular, 3.1 arcsec (VCL) and 1.3 arcsec (ICESat) pointing bias knowledge can be achieved using a 3-deg maneuver; 1.9 (VCL) and 0.8 (ICESat) arcsec knowledge can be achieved with a 5-deg amplitude maneuver. This approach has minimal impact on mission resources and causes no degradation of primary science data acquisition. Furthermore, it is relatively insensitive to uncertainties in sea-surface height, slope, or roughness. The method is also capable of tuning prelaunch thermal pointing variation models where parameters governing the size, direction, and phase of the pointing variations are simultaneously estimated with range, roll, and pitch biases. Scheduled recalibrations over the mission lifetime will support long period monitoring of mission pointing changes because of the aging of systems and long period environmental influences. As the system errors become better known, the calibration maneuver profile can be modified from the nominal profile presented here to better address the observability of these error signals. Finally, the system implementation of the measurement model has been done such that it will support a generic surface model grid. In this way the system can be used to reduce laser-altimeter range data over any known surface where a model can be supplied. This will be quite useful for data analysis over independently mapped and well-known surfaces.

Appendix: Laser-Altimeter Range Measurement Model Algorithm

The laser range measurement is a two-way measurement. In other words, the laser pulse is transmitted from the satellite and is bounced off of the planet surface before being received back at the satellite. To compute our estimate of this two-way range, we first model the downrange by performing a rigorous, iterative light time solution. We start the modeling at the laser optical center at transmit time because the measurement is tagged at transmit time and more importantly because the path of the two-way range depends very heavily upon the orientation of the laser at transmit time. The downleg light-time solution yields the location and the time of the surface bounce point. Starting from this time and location, the up-leg range is traced back up to the satellite. This also requires an iterative light-time solution to determine a satellite receive time. The receive time determines the satellite position at the end of the two-way range. The distance from the bounce point to this ending satellite position must match the time of travel from the bounce point time tag to the receive time tag.

The light-time solution on the downleg is more difficult than it is on the up leg. Because of this, some details of the downleg computations are given immediately before all of the steps are summarized. On the downleg we want to find the intersection between a straight line and a complicated surface. The problem is made more difficult by the fact that the line is only straight in the IRF and also because the complicated surface is changing its orientation in inertial space. On each iteration we tackle this problem by first making a bounce point guess in the IRF along the line from the satellite position at transmit time. The location of the guess on the line also yields a guess for the bounce point time tag. With the bounce point time tag the IRF bounce point coordinates can be converted to ECF. The ECF Cartesian coordinates are easily converted to geodetic. Given geodetic coordinates and the bounce point time tag, the static surface height above the ellipsoid and the time-varying surface displacement can be computed. It can then be seen if the bounce point guess is above or below the surface and the distance along the line from the satellite can be altered accordingly. This yields the bounce point coordinates on the next iteration.

Of course, it is important to refine the bounce point time tag very well before proceeding to the up-leg computations. However, the location of the bounce point on the first iteration is computed in such a way as to guarantee that the associated bounce point time tag is good to well under 0.1 ms. The computed value is good enough so that the rotation matrices needed for IRF to ECF coordinates do not need to be recomputed on subsequent iterations. In addition, the initial bounce point location and time are sufficient so that time-varying effects such as tides do not need to be recomputed as bounce point estimates and time tags change. The first iteration bounce point coordinates are found by finding the intersection of the line with an ellipsoid that approximates the Earth. This intersection is computed in the IRF; however, our choice of inertial coordinate system (e.g., J2000) guarantees that the ellipsoid will be somewhat misaligned with the Earth at measurement time. However, the orientation is sufficient enough for initial bounce point estimation.

1) The optical center and the pointing of the laser altimeter are both computed in the IRF at instrument transmit time:

$$\boldsymbol{XOP}^{\mathrm{T}}_{\mathrm{IRF}} = \boldsymbol{XSC}^{\mathrm{T}}_{\mathrm{IRF}} + \boldsymbol{XCM}^{\mathrm{T}}_{\mathrm{IRF}}$$

$$\hat{\boldsymbol{p}}^{\mathrm{T}}_{\mathrm{IRF}} = R^{\mathrm{T}}_{\mathrm{SBF}\rightarrow\,\mathrm{IRF}} R^{\mathrm{T}}_{\mathrm{SBFC}\rightarrow\,\mathrm{SBF}} R^{\mathrm{T}}_{\mathrm{Laser}\rightarrow\,\mathrm{SBFC}} \begin{bmatrix} 0 \\ 0 \\ -1 \end{bmatrix} \tag{A1}$$

2) The direction cosines of the IRF pointing unit vector are used to form the equation of a line. Coupled with the equation of an ellipsoid, one can then solve for the intersection of the observation line of sight with the ellipsoid. The ellipsoid intersection is then used as the first guess for the location of the altimeter bounce point. Also, one could simply use the ellipsoid height of the spacecraft along the pointing vector for an initial guess: $\boldsymbol{XB}^{B}_{\mathrm{IRF}}$.

3) The bounce point time is computed using the range correction for atmospheric refraction:

$$T^{B} = T^{\mathrm{T}} + \left(\left|\boldsymbol{XOP}^{\mathrm{T}}_{\mathrm{IRF}} - \boldsymbol{XB}^{B}_{\mathrm{IRF}}\right| + \Delta\rho_{\mathrm{atm}}\right) / c \tag{A2}$$

4) The IRF bounce point position is then rotated to ECF: $\boldsymbol{XB}^{B}_{\mathrm{ECF}}$.

5) Geodetic coordinates are then computed from the current estimate of the bounce point. These geodetic coordinates and the bounce point time are used to compute the surface including all site displacement effects (e.g., Earth and ocean tides, pole tide, ocean loading): $\boldsymbol{XS}^{B}_{\mathrm{ECF}}$.

6) The distance between the surface and the first guess bounce point is then computed:

$$d = \left|\boldsymbol{XS}^{B}_{\mathrm{ECF}} - \boldsymbol{XB}^{B}_{\mathrm{ECF}}\right| \tag{A3}$$

(The sign of d must be assigned depending on whether the surface is below or above the bounce point.)

7)If d has converged (i.e., d is less than some ε), then the bounce point location and time have been found. If not, then a new bounce point guess is computed as follows and iterated until convergence:

$$\boldsymbol{XB}^{B\,(n+1)}_{\mathrm{IRF}} = \boldsymbol{XB}^{B\,(n)}_{\mathrm{IRF}} - d\left(-\hat{\boldsymbol{p}}^{\mathrm{T}}_{\mathrm{IRF}}\right) \tag{A4}$$

8) The geometric transmit leg range is then computed using the converged bounce point:

$$\rho^{\mathrm{T}} = \left|\boldsymbol{XOP}^{T}_{\mathrm{IRF}} - \boldsymbol{XB}^{B}_{\mathrm{IRF}}\right| \tag{A5}$$

9) Now, the receive spacecraft position in IRF is computed using an iterative light-time solution, given the IRF bounce point position. The first guess of the receive time is

$$T^{R} = T^{\mathrm{T}} + 2\left(\rho^{\mathrm{T}} + \Delta\rho_{\mathrm{atm}}\right) / c \tag{A6}$$

10) Once converged, the optical center of the instrument at the receive time is then computed as

$$\boldsymbol{XOP}^{R}_{\mathrm{IRF}} = \boldsymbol{XSC}^{R}_{\mathrm{IRF}} + \boldsymbol{XCM}^{R}_{\mathrm{IRF}} \tag{A7}$$

11) The laser two-way range is then computed as

$$\rho_{\text{2-way}} = \left|\boldsymbol{XOP}^{R}_{\mathrm{IRF}} - \boldsymbol{XB}^{B}_{\mathrm{IRF}}\right| + \rho^{\mathrm{T}} + 2\Delta\rho_{\mathrm{atm}} + 2\Delta\rho_{\mathrm{bias}} \tag{A8}$$

12) The partial derivatives of the range measurement with respect to the spacecraft position and range biases are rigorously computed from the preceding equation. The partials of the measurement with respect to spacecraft attitude corrections and laser pointing are numerically approximated because of the additional complexity of the surface model.

Acknowledgments

The authors wish to thank the VCL and ICESat programs for the support we received in completing this research. The authors also wish to thank Bryan Blair and Claudia Carabajal for their many technical contributions.

References

[1]Garvin, J., Bufton, J., Blair, J., Harding, D., Luthcke, S., Frawley, J., and Rowlands, D., "Observations of the Earth's Topography from the Shuttle Laser Altimeter (SLA): Laser Pulse Echo-Recovery Measurements of Terrestrial Surfaces," *Physics and Chemistry of the Earth*, Vol. 23, No. 9–10, 1998, pp. 1053–1068.

[2]Smith, D. E., Zuber, M. T., Frey, H. V., Garvin, J. B., Head, J. W., Muhleman, D. O., Pettengill, G. H., Phillips, R. J., Solomon, S. C., Zwally, H. J., Banerdt, W. B., and Duxbury, T. C., "Topography of the Northern Hemisphere of Mars from the Mars Orbiter Laser Altimeter," *Science*, Vol. 279, March 1998, pp. 1686–1692.

[3]Vaughn, C. R., Bufton, J. L., Krabill, W. B., and Rabine, D., "Georeferencing of Airborne Laser Altimeter Measurements," *International Journal of Remote Sensing*, Vol. 17, No. 11, 1996, pp. 2185–2200.

[4]Hofton, M. A., Blair, J. B., Minster, J.-B., Ridgway, J. R., Williams, N. P., Bufton, J. L., and Rabine, D. L., "An Airborne Scanning Laser Altimetry Survey of Long Valley, California," *International Journal of Remote Sensing* (to be published).

[5]Dubayah, R., Blair, J. B., Bufton, J. L., Clark, D. B., JaJa, J., Knox, R., Luthcke, S. B., Prince, S., and Weishampel, J., "The Vegetation Canopy Lidar Mission," *Land Satellite Information in the Next Decade II: Sources and Applications*, American Society for Photogrammetry and Remote Sensing, Bethesda, MD, Dec. 1997, pp. 100–112.

[6]Rim, H. J., Webb, C., and Schutz, B. E., "Analysis of GPS and Satellite Laser Ranging (SLR) Data for ICESat Precision Orbit Determination," American Astronautical Society, AAS Paper 99-146, Feb. 1999.

[7]Gardner, C. S., "Ranging Performance of Satellite Laser Altimeters," *IEEE Transactions on Geoscience and Remote Sensing*, Vol. 30, No. 5, 1992, pp. 1061–1072.

[8]Pavlis, D. E., Moore, D., Luo, S., McCarthy, J. J., and Luthcke, S. B., "GEODYN Operations Manual: 5 Volumes," Raytheon ITSS, Greenbelt, MD, Dec. 1999.

[9]Nishihama, M., "ERODYN Program Mathematical Formulation," Hughes STX Corp., Lanham, MD, Sept. 1993.

[10]Lillibridge, J., "Real-Time Altimetry from ERS-2," *Proceedings of the 3rd European Remote Sensing Symposium*, edited by T. D. Guyenne and D. Danesy, ESA, Noordwijk, The Netherlands, 1999, pp. 18–21.

[11]Kraus, E. B., and Businger, J. A., *Atmosphere-Ocean Interaction*, 2nd ed., Oxford Univ. Press, New York, 1994, p. 132.

[12] Stewart, R. H., Methods of Satellite Oceanography, Univ. of California Press, Los Angeles, 1985, p. 19.

[13] Yi, Y., "Determination of Gridded Mean Sea Surface from TOPEX, ERS-1 and GEOSAT Altimeter Data," Ohio State Univ., Rept. 434, Columbus, OH, Dec. 1995.

[14] Wunsch, C., and Stammer, D., "The Global Frequency-Wavenumber Spectrum of Oceanic Variability Estimated from TOPEX/POSEIDON Altimetric Measurements," *Journal of Geophysical Research*, Vol. 100, No. C12, 1995, pp. 24,895–24,910.

[15] Shum, C. K., Woodworth, P. L., Andersen, O. B., Egbert, G. D., Francis, O., King, C., Klosko, S. M., LeProvost, C., Li, X., Molines, J., Parke, M. E., Ray, R. D., Schlax, M. G., Stammer, D., Tierney, C., Vincent, P., and Wunsch, C. I., "Accuracy Assessment of Recent Ocean Tide Models," *Journal of Geophysical Research*, Vol. 102, No. C11, 1997, pp. 25,173–25,194.

[16] Fu, L.-L., Christensen, E. J., Yamarone, C. A., Jr., Lefebvre, M., Menard, Y., Dorrer, M., and Escudier, P., "TOPEX/POSEIDON Mission Overview," *Journal of Geophysical Research*, Vol. 99, No. C12, 1994, pp. 24,369–24,381.

[17] Fu, L.-L., and Pihos, G., "Determining the Response of Sea Level to Atmospheric Pressure Forcing Using TOPEX/POSEIDON Data," *Journal of Geophysical Research*, Vol. 99, No. C12, 1994, pp. 24,633–24,642.

[18] Schrama, E. J. O., and Ray, R. D., "A Preliminary Tidal Analysis of TOPEX/POSEIDON Altimetry," *Journal of Geophysical Research*, Vol. 99, No. C12, 1994, pp. 24,799–24,808.

C. A. Kluever
Associate Editor